Acta Pharmaceutica Sinica B 2022;12(11):4249–4261

Chinese Pharmaceutical Association
Institute of Materia Medica, Chinese Academy of Medical Sciences

Acta Pharmaceutica Sinica B

www.elsevier.com/locate/apsb
www.sciencedirect.com

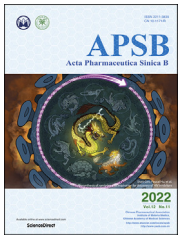

ORIGINAL ARTICLE

Site-selective oral delivery of therapeutic antibodies to the inflamed colon *via* a folic acid-grafted organic/inorganic hybrid nanocomposite system

Sang Hoon Lee, Jae Geun Song, Hyo-Kyung Han*

College of Pharmacy, Dongguk University-Seoul, Goyang 10326, South Korea

Received 19 December 2021; received in revised form 7 April 2022; accepted 18 April 2022

KEY WORDS

Infliximab;
Aminoclay;
Colonic delivery;
TNF-α;
Inflammation;
Folate receptor;
Antibody;
Nanocomposite

Abstract This study aimed to develop a pH-responsive folic acid-grafted organic/inorganic hybrid nanocomposite system for site-selective oral delivery of therapeutic antibodies. A folic acid-grafted aminoclay (FA-AC) was prepared *via* an *in situ* sol–gel method. Then, a drug-loaded nanocomplex was prepared *via* the electrostatic interaction of FA-AC with infliximab (IFX), a model antibody, and coated with Eudragit® S100 (EFA-AC-IFX). FA-AC exhibited favorable profiles as a drug carrier including low cytotoxicity, good target selectivity, and capability to form a nanocomplex with negatively charged macromolecules. A pH-responsive FA-AC-based nanocomplex containing IFX (EFA-AC-IFX) was also obtained in a narrow size distribution with high entrapment efficiency (>87%). The conformational stability of IFX entrapped in EFA-AC-IFX was well maintained in the presence of proteolytic enzymes. EFA-AC-IFX exhibited pH-dependent drug release, minimizing premature drug release in gastric conditions and the upper intestine. Accordingly, oral administration of EFA-AC-IFX to colitis-induced mice was effective in alleviating the progression of ulcerative colitis, while oral IFX solution had no efficacy. These results suggest that a pH-responsive FA-AC-based nanocomposite system can be a new platform for the site-selective oral delivery of therapeutic antibodies.

*Corresponding author. Tel.: +82 31 9615217.
E-mail address: hkhan@dongguk.edu (Hyo-Kyung Han).

Peer review under responsibility of Chinese Pharmaceutical Association and Institute of Materia Medica, Chinese Academy of Medical Sciences

https://doi.org/10.1016/j.apsb.2022.06.006

1. Introduction

Therapeutic monoclonal antibodies are widely used for the treatment of various diseases including cancer, inflammation, and autoimmune diseases[1,2]. Accordingly, the global market for therapeutic antibodies has rapidly grown since the first approval of a monoclonal antibody (Orthoclone OKT_3) by the US Food and Drug Administration (FDA) in 1986[3]. More than 50 monoclonal antibody-based products have been approved, and over 500 monoclonal antibody-based therapies are under clinical development[4]. However, monoclonal antibodies are mainly available in injectable formulations, leading to low patient compliance and unintended adverse effects[5,6]. Therefore, more patient-friendly drug delivery systems for therapeutic antibodies are in high demand.

Among noninvasive dosage forms, oral delivery systems provide some advantages including ease of self-medication, high patient compliance, and low manufacturing cost[7,8]. However, there are many barriers to oral delivery of antibodies including their physicochemical instability in the gastric environment, susceptibility to enzymatic degradation, and low membrane permeability[9,10]. To overcome these barriers, various formulation approaches have been explored including the use of organic/inorganic nanocomposites, hydrogels, polymeric nanoparticles, and porous silicon nanoparticles[11–17]. For example, Carrillo-Conde et al.[17] fabricated a pH-responsive hydrogel system for oral delivery of monoclonal antibodies. When loaded with anti-tumor necrosis factor (TNF)-α antibodies, this hydrogel system enhanced the gastrointestinal (GI) stability and the systemic circulation of these biologically active antibodies in rats[17]. However, increased systemic circulation of immunosuppressive monoclonal antibodies may lead to undesirable adverse effects including hypersensitivity, immunodeficiency-related infections and malignancies, and the generation of antibodies against these drugs[18]. Therefore, effective oral and site-selective local delivery of therapeutic antibodies to pathologically functional cells could be beneficial to reduce systemic side effects and improve patient compliance.

Aminoclay (AC) is a derivative of highly disordered talc-like 2:1 trioctahedral magnesium phyllosilicates with covalently attached aminopropyl moieties[19]. AC is water-soluble and positively charged as dispersed in water. It exhibits many favorable properties as a drug carrier including its low cytotoxicity, low risk of long-term accumulation, and reversible effect on tight junction opening[20–23]. Furthermore, the formation of an AC-protein nanocomplex effectively improves the GI stability and intestinal permeability of entrapped proteins[20–22]. AC also has a large surface area, allowing surface modification with various targeting ligands. Since interactions between the targeting ligands of drug carriers and the specific receptors on the target cell surface can promote site-selective drug delivery, surface modifications of AC with certain targeting ligands can create effective site-selective drug delivery carriers for macromolecules. Among targeting ligands, folic acid (FA) plays an essential role in cell survival, and has a high binding affinity ($K_d \approx 10^{-9} - 10^{-10}$ M) to folate receptors (FRs)[24–26], a biomarker for cancers and inflammatory diseases. Among FR isoforms, folate receptor-β (FR-β) is highly expressed in activated macrophages[27,28]; in contrast, it has very low or undetectable expression in resting/quiescent macrophages or any other normal cells[29]. Owing to this differential expression of FR-β, surface modifications of AC with FA should be a promising approach to develop a new site-selective delivery carrier targeting activated macrophages that are the key mediators of many inflammatory diseases.

Infliximab (IFX), a chimeric human-mouse IgG monoclonal antibody to TNF-α, is used for the treatment of chronic inflammatory disorders including ulcerative colitis, Crohn's disease, and rheumatoid arthritis[30]. IFX is effective to reduce histological disease activity and restore gut barrier function[31,32]. While IFX interacts directly with soluble and membrane TNF-α for blocking their effects, various mechanisms have been proposed to clarify the efficacy of IFX in addition to TNF-α neutralization[31–33]. For example, Assas et al.[33] have demonstrated the anti-inflammatory effects of IFX in mice although IFX did not bind directly to TNF-α. While the mechanism of action of IFX is not fully defined yet, it is clear that its efficacy cannot be explained by TNF-α neutralization alone[33,34]. In current medical practice, IFX is administered by intravenous injection or subcutaneous injection, resulting in low patient compliance and systemic immunosuppression[35,36]. Considering that IFX induces a potent local effect and its gut concentrations may correlate well with a clinical response[34], the effective oral and local delivery of IFX to the inflamed colon could be beneficial in improving the patient compliance with reduced systemic adverse effect.

The present study aimed to develop an FA-grafted AC (FA-AC)-based-nanocomposite system to establish a new platform for effective oral and site-selective delivery of therapeutic monoclonal antibodies (Scheme 1). First, FA-AC was prepared as a new drug delivery carrier for therapeutic antibodies *via* an *in situ* sol−gel method. The core nanocomplex of FA-AC and IFX (a model drug) was prepared *via* spontaneous co-assembly and then coated with Eudragit® S100, a pH-sensitive polymer. The structural and *in vitro*/*ex vivo* characteristics of the developed delivery system were evaluated using various analytical methods, and the *in vivo* therapeutic effects were also assessed in a mouse model of colitis.

2. Materials and methods

2.1. Materials

Infliximab, fluorescein isothiocyanate (FITC)-labeled bovine serum albumin (FITC-BSA), dimethyl sulfoxide (DMSO), folic acid (FA), hematoxylin solution, eosin Y solution, myeloperoxidase (MPO) colorimetric activity assay kit, and 3-aminopropyltriethoxysilane (APTES, 99%) were purchased from Sigma−Aldrich (St. Louis, MO, USA). Eudragit® S100 was obtained from Evonik Korea Ltd (Seoul, Korea). Dulbecco's modified Eagle's medium (DMEM), RPMI 1640 (without folic acid), nonessential amino acids, fetal bovine serum (FBS), antibiotics (penicillin-streptomycin), non-reducing lithium dodecyl sulfate (LDS) sample buffer (4×), PageRuler™ prestained protein ladder, Pierce™ bicinchoninic acid (BCA) protein assay kit, polyvinylidene fluoride (PVDF) membrane, folate receptor-β (FOLR2) polyclonal antibody, β-tubulin monoclonal antibody, anti-rabbit secondary antibody, and all other reagents used in cell culture studies were obtained from Thermo Fisher Scientific (Waltham, MA, USA). In addition, 4′,6-diamidino-2-phenylindole (DAPI), an interleukin (IL)-6 enzyme-linked immunosorbent assay (ELISA) kit, and a TNF-α ELISA kit were purchased from Invitrogen (Waltham, MA, USA). Twelve percent Mini-PROTEAN® TGX™ precast protein gels, 10× tris-glycine buffer, 10× tris-glycine-sodium dodecyl sulphate (SDS) buffer, Clarity™ Western ECL substrate, blotting-grade blocker, 10% Tween 20 solution, and Coomassie brilliant blue R-250 staining solution were purchased

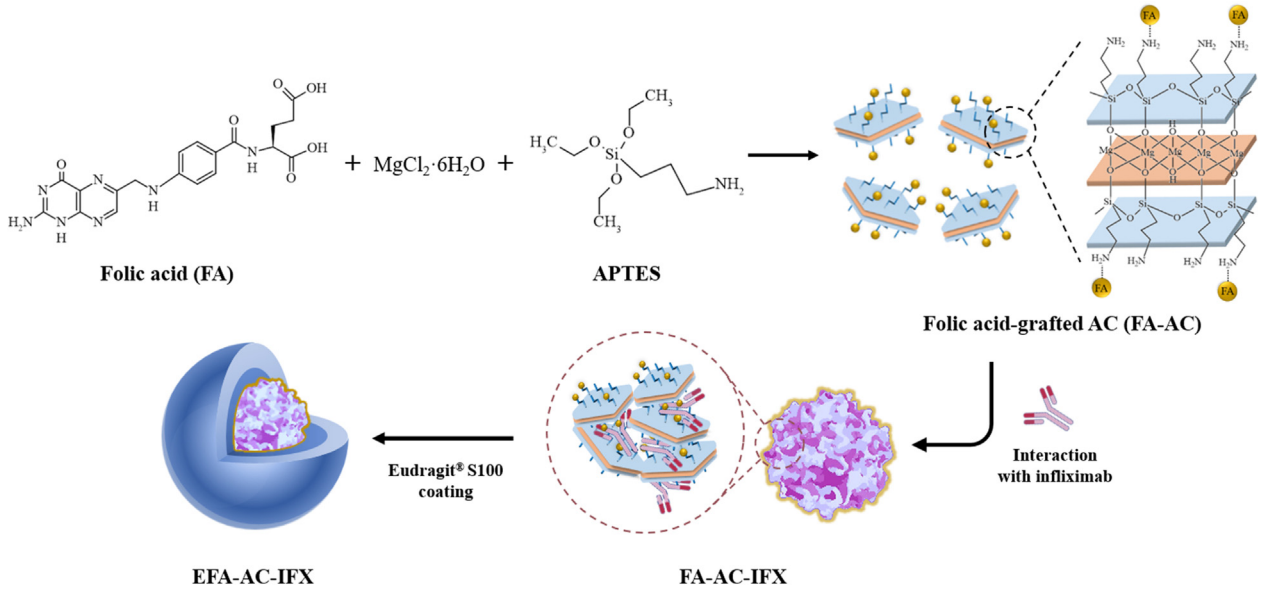

Scheme 1 Schematic illustration of a pH-responsive FA-grafted organic/inorganic hybrid nanocomposite system for site-selective oral delivery of IFX.

from Bio-Rad (Hercules, CA, USA). Magnesium chloride hexahydrate (98%) and other inorganic salts were purchased from Junsei Chemical Co., Ltd (Tokyo, Japan). All other chemicals and reagents were high-performance liquid chromatography (HPLC) grade.

2.2. *Cells*

Caco-2 cells (human epithelial colorectal adenocarcinoma cells) and RAW264.7 cells (murine macrophage cell line) were purchased from the Korean Cell Line Bank (Seoul, Korea). Caco-2 cells were grown in DMEM containing 10% FBS, 1% nonessential amino acids, and 1% antibiotics. RAW264.7 cells were grown in DMEM containing 10% FBS and 1% antibiotics. Cells were incubated at 37 °C in an atmosphere of 5% CO_2 and 90% relative humidity.

2.3. *Preparation of FA-AC*

FA-AC was prepared *via* an *in situ* sol−gel method[23,37]. Briefly, $MgCl_2 \cdot 6H_2O$ (8.4 g) was dissolved in ethanol (100 mL) and then mixed with FA (50 mg) dissolved in a mixture of ethanol and DMSO (100 mL, 25% DMSO). APTES (13 mL) was added dropwise to the reaction mixture under the stirring at 250 rpm (Digital hotplate stirrer, Daihan Scientific, Wonju, Korea), resulting in the rapid formation of yellow precipitate. The mixture was stirred overnight to ensure sufficient equilibrium time for the formation of FA-AC. The resulting precipitate was separated by centrifugation, washed five times with ethanol, and dried in an oven at 40 °C. The amount of FA in FA-AC was determined using microplate reader (SpectraMax M2e, Molecular Devices, San Jose, CA, USA) at 360 nm[38]. The amount of FA in 1 mg of FA-AC was 10.2 μg.

2.4. *Preparation of a drug-loaded FA-AC nanocomplex*

For exfoliation of FA-AC, the bulk powder was dispersed in water under ultrasonication for 10 min. An aqueous solution of IFX was added dropwise to an equal volume of exfoliated FA-AC suspension in water at a drug/clay ratio of 1:4 (*w*/*w*). After stirring for 4 h at room temperature, the resulting product was separated by centrifugation at 20,000×*g* for 15 min at 4 °C. Subsequently, the obtained FA-AC-IFX underwent surface coating with Eudragit® S100. The aqueous suspension of FA-AC-IFX (1 mg/mL) was added dropwise into an equal volume of 0.2% Eudragit® S100 dissolved in ethanol while stirring at 250 rpm. The resultant Eudragit® S100-coated nanocomplex (EFA-AC-IFX) was separated by centrifugation (20,000×*g*) at 4 °C for 15 min. FA-AC-IFX and EFA-AC-IFX were freeze-dried with 2% trehalose. For the comparison, AC-based nanocomplex (EAC-IFX) was also prepared following the same procedures described above where FA-AC was replaced by AC. For bio-imaging studies, a fluorescence-labeled nanocomplex was fabricated with replacing IFX by FITC-BSA.

2.5. *Physicochemical and structural characterization of the nanocomplex*

The particle size and zeta potential of nanoparticles were measured by dynamic light scattering (DLS) using a Zetasizer Nano-ZS90 (Malvern Instruments, Malvern, UK). The polydispersity index (PDI) was also measured as a dimensionless number indicating the size distribution. The entrapment efficiency (EE) was calculated by the following Eq. (1):

$$\text{Entrapment efficiency}\ (\%) = \frac{\text{Drug amount in nanocomposites}}{\text{Drug amount initially added}} \times 100 \quad (1)$$

The structural characterization was also performed using Fourier transform infrared spectroscopy (FT-IR) (Nicolet™ iS™ 5; Thermo Fisher Scientific, Waltham, MA, USA) with a ZnSe crystal accessory. The FT-IR spectrum of each sample was measured over a wavenumber range of 4000−500 cm^{-1} with 64 scans at resolution of 4 cm^{-1}. X-ray diffraction (XRD) patterns were examined using an X-ray diffractometer (X'Pert APD,

PHILIPS, Netherland) with CuKα radiation at 40 kV and 25 mA. The diffraction patterns were obtained over a 2θ range of 2°−70° using a step size of 0.04° at a scan speed of 2 s/step. The morphological characteristics of nanocomplex were also monitored by transmission electron microscopy (TEM) (JEM-2100F; JEOL Ltd., Tokyo, Japan). XRD analysis and TEM analysis were performed at the Korean Basic Science Institute (Daegu Center and Chuncheon Center, Korea).

2.6. Circular dichroism (CD) analysis and sodium dodecyl sulphate−polyacrylamide gel electrophoresis (SDS-PAGE)

CD analysis and SDS-PAGE were used to examine the structural stability of IFX entrapped in nanocomplex. Far UV CD spectra were collected using the Chirascan™-Plus Spectrometer (Applied Photophysics, Surrey, UK). Wavelength spectra were collected from 200 to 260 nm at 25 °C with a bandwidth of 1 nm and a light path length of 0.5 mm[39].

SDS-PAGE was performed under non-reducing conditions using Mini-PROTEAN® TGX™ (Bio-Rad Laboratories Inc., Hercules, CA, USA) gel apparatus. Samples were diluted with equal volumes of non-reducing SDS-PAGE sample buffer and incubated at 95 °C for 5 min. Prestained protein ladder (5 μL) and each sample (10 μL) were loaded into the wells of 12% Mini-PROTEAN® TGX™ precast protein gels. Gels were run at 30 mA for 60 min and then stained with Coomassie blue solution for 15 min and washed with distilled water. Protein bands were visualized by ChemiDoc Imaging System (Bio-Rad, Hercules, CA, USA).

2.7. Protection against enzymatic degradation

The structural stability of IFX entrapped in EFA-AC-IFX was examined in simulated gastric fluid (SGF) and simulated intestinal fluid (SIF). SGF (pH 1.2) was composed of 50 μg/mL pepsin, 0.2% sodium chloride, and 0.7% hydrochloric acid. SIF (pH 7.4) was composed of 200 μg/mL trypsin, 50 mmol/L potassium dihydrogen phosphate, and 0.16% sodium hydroxide. After incubating EFA-AC-IFX in SGF or SIF at 37 °C for 2 h, the enzymatic reaction was terminated by adding either 0.2 mmol/L NaOH into SGF or 0.1 M HCl into SIF. Nanoparticles were collected by centrifugation (20,000×g) for 10 min, and IFX in nanoparticles was extracted in a phosphate buffer (pH 7.4) for 3 h. The structural stability of IFX extracted from nanoparticles was examined and compared with that of native IFX using CD spectroscopy and SDS-PAGE.

2.8. In vitro drug release studies

The pH-dependent drug release from the nanocomplex was examined in a pH transition buffer system where the pH of the release medium was gradually changed to reflect the pH changes (pH 1.2, 7.2, and 5.5) from the stomach to the lower intestine to the inflamed colon[40,41]. The pH of release medium was adjusted to reach the designated pH using 0.1 mol/L hydrochloric acid or a 0.21 mol/L tribasic sodium phosphate solution. Each nanocomplex (equivalent to 0.1 mg/mL of IFX) was exposed to 75 mL of 0.1 mol/L hydrochloric acid and incubated for 2 h in a shaking water bath (100 rpm) at 37 °C. Then, 25 mL of 0.21 mol/L tribasic sodium phosphate was added to the release medium for the transition to pH 7.2 and incubated for 8 h. The pH of the release medium was adjusted to 5.5 by adding 1 mL of 1 mol/L hydrochloric acid and incubated for 4 h. At the predetermined time points, samples (200 μL) were withdrawn, and the release medium was replenished with an equal volume of fresh medium. The collected samples were centrifuged at 20,000×g at 4 °C for 10 min. Then, the drug content in the supernatant was analyzed by BCA protein assay kit (Thermo Fisher Scientific, Waltham, MA, USA).

2.9. Cytotoxicity studies

The cytotoxicity of FA-AC was evaluated in RAW264.7 cells and Caco-2 cells. Cells were seeded in 96-well plates at a density of 1×10^4 cells per well, and incubated for 24 h. Then, cells were treated with FA-AC solution over the concentration range of 1−1000 μg/mL and incubated for 48 h. At the end of incubation, the medium was replaced by 100 μL of thiazolyl blue tetrazolium bromide solution (0.5 mg/mL in PBS) and incubated for 4 h. Finally, the medium was removed, and 100 μL of DMSO was added to each well to dissolve the formazan crystals. The absorbance of each sample was measured at 550 nm using a microplate reader (SpectraMax M2e, Molecular Devices, San Jose, CA, USA).

2.10. Expression of folate receptor-β (FR-β) in RAW264.7 cells

The expression level of FR-β in RAW264.7 cells was determined by Western blotting. After incubating cells in culture medium with/without lipopolysaccharide (LPS; 100 ng/mL) for 24 h, cell lysates were prepared with radioimmunoprecipitation assay (RIPA) buffer supplemented with protease inhibitors. The amount of proteins in the cell lysates was determined by a BCA protein assay. The aliquots (20 μg) of protein from each sample were loaded on 12% Mini-PROTEAN® TGX™ precast protein gels (Bio-Rad, Hercules, CA, USA). After SDS-PAGE and electroblotting, membranes were treated for 1 h with 5% skim milk in PBS with 0.1% Tween 20 (PBST) to block nonspecific binding and then incubated with an FR-β primary antibody for 12 h at 4 °C. Membranes were washed with PBST and then incubated with horseradish peroxidase-conjugated secondary antibody for 1 h at room temperature. Protein bands were visualized using the enhanced chemiluminescent (ECL) detection system (GE Healthcare, Chalfont St Giles, UK). β-Tubulin was used as the loading control.

2.11. Cellular uptake studies

To evaluate the targeting effect to macrophages overexpressing FR-β, the cellular uptake characteristics of each nanocomplex were evaluated in RAW264.7 cells with and without LPS activation. RAW 264.7 cells were seeded into 12-well plates at a density of 3×10^5 cells per well and incubated in the presence and absence of LPS (100 ng/mL) for 24 h. At the end of incubation, the medium was removed, and cells were incubated in serum-free RPMI 1640 (no FA) for 1 h. Then, each fluorescence-labeled nanocomplex (EFA-AC-FITC-BSA or EAC-FITC-BSA) was added to the cells at a concentration equivalent to 0.2 mg/mL of FITC-BSA and incubated for 2 h. After removing the drug solution, cells were washed three times with ice-cold PBS. Cells were detached with 0.25% trypsin−0.02% EDTA, washed with PBS, and re-suspended in 0.5 mL PBS for flow cytometry analysis. The mean fluorescence intensity was measured using BD FACS Aria III (BD Biosciences, San Jose, CA, USA), as previously reported[20]. Cells were analyzed with excitation at 488 nm and emission at 522 nm. To confirm the interaction of the nanocomplex with FR-β, the cellular uptake of the nanocomplex was also evaluated after pretreatment with FA. Cells were pre-

incubated with serum-free RPMI 1640 containing 1 mmol/L FA for 1 h. At the end of incubation, the medium was removed and cells were washed three time with ice-cold PBS. Then, the cellular uptake of the nanocomplex was evaluated following the same procedures as described above.

2.12. Evaluation of intracellular distribution by confocal laser scanning microscopy (CLSM)

The intracellular localization of nanoparticles was examined by CLSM. Briefly, RAW264.7 cells were seeded on a coverslip placed in 24-well plates at a density of 5×10^4 cells per well and incubated in the presence and absence of LPS (100 ng/mL) for 24 h. At the end of incubation, the medium was removed, and cells were incubated with serum-free RPMI 1640 (no FA) for 1 h. Then, each nanocomplex was added to the cells at a concentration equivalent to 50 μg/mL FITC-BSA and incubated for 2 h. After removing the drug solution, cells were washed three times with ice-cold PBS and fixed in 4% paraformaldehyde. The nuclei were stained with DAPI (10 μg/mL). The intracellular distribution of each nanocomplex was visualized using a Nikon C1 confocal laser scanning microscope with EZ-C1 software (Nikon, Tokyo, Japan). The intracellular localization of nanoparticles was also evaluated after pretreatment with FA to confirm the interaction of the nanocomplex with FR-β.

2.13. Animal studies

All animal studies were conducted in accordance with the "Guiding Principles in the Use of Animals in Toxicology" adopted by the Society of Toxicology (USA), and the study protocol was approved by the Review Committee of Dongguk University (IACUC-2019-034-2). Eight-week-old male C57BL/6 (24 ± 2 g) mice were purchased from Orient Bio Inc (Seongnam, Korea). C57BL/6 mice were kept under standard conditions at 21−22 °C under a 12-h light/dark cycle for 7 days before the experiments.

2.14. Colonic absorption study in dextran sulfate sodium (DSS)-induced colitis mice

The colonic accumulation of orally administered nanocomplex was evaluated in DSS-induced colitis mice and healthy mice[42]. Colitis was induced in mice by administering 2% DSS in drinking water for consecutive 7 days. Age matched mice receiving normal tap water were used as controls (healthy mice). After fasting for 12 h, DSS-induced colitis mice and healthy mice were orally administered each nanocomplex (a dose equivalent to 10 mg/kg of FITC-BSA). Mice were sacrificed 12 h after dosing, and their colons were excised immediately after laparotomy. The colons were washed with ice-cold PBS to remove luminal contents. The colons were fixed with 4% paraformaldehyde for 24 h and placed in 30% sucrose solution for 24 h at 4 °C. Then, the colonic tissues were cryosectioned and examined by confocal microscopy (Nikon C1, Nikon, Tokyo, Japan) to visualize the localization of FITC-BSA. In addition, to quantify the FITC-BSA content in the colon, 50 mg of the colonic segments was homogenized in 0.5 mL of RIPA buffer and centrifuged at 15,000×g for 15 min. The FITC-BSA content in supernatant was determined by using a microplate reader (SpectraMax M2e, Molecular Devices, San Jose, CA, USA) with excitation at 488 nm and emission at 522 nm.

2.15. In vivo efficacy studies

The efficacy of orally administered IFX-loaded nanocomplex was evaluated in DSS-induced colitis mice. Mice were randomly divided into seven different treatment groups (4 mice per group): healthy control, colitis control, PBS-treated, empty vehicle-treated, IFX-treated, EAC-IFX-treated, and EFA-AC-IFX-treated groups. First, colitis was induced in mice by administering 2% DSS-supplemented drinking water for 7 days (Days 0−6). Each treatment group was administered 200 μL of PBS, empty vehicle, IFX (10 mg/kg), or IFX-loaded nanocomplex (equivalent to 10 mg/kg of IFX) orally once daily for 8 consecutive days (Days 0−7). On Day 7, 2% DSS-supplemented drinking water was replaced by normal tap water and maintained for 2 days. The healthy control received normal tap water throughout the whole study. On Day 9, mice were sacrificed and their entire colons were excised to evaluate the therapeutic efficacy in each treatment group. The colon length was measured, and the colon was washed with ice-cold PBS. Then, two pieces of the distal sections (0.5 cm in length) were used for histological assessment. The remaining colonic tissue samples were used to determine the levels of MPO activity and pro-inflammatory cytokines. Changes in body weight, stool consistency, and rectal bleeding were also monitored daily throughout the study period. The disease activity index (DAI) was evaluated using the summed score of three parameters (body weight loss, stool consistency, and rectal bleeding) as previously described[43].

2.16. Histological analysis

Histological analysis of colonic tissues was performed using hematoxylin-eosin (H&E) staining. Colonic tissues were fixed in 4% paraformaldehyde and embedded in paraffin. The embedded colons were then cut into 5-μm-thick sections using a microtome (Leica, Wetzlar, Germany), stained with H&E, and scanned using an Eclipse Ti−U inverted microscope (Nikon, Tokyo, Japan). The severity of colitis in each colonic section was evaluated by monitoring the mucosal features, such as epithelial damage, mucosal edema, and infiltration of inflammatory cells[42,44].

2.17. Evaluation of myeloperoxidase (MPO) activity and pro-inflammatory cytokine levels

MPO activity was measured using an MPO colorimetric activity assay kit (Sigma−Aldrich). Briefly, the colonic tissues (50 mg) were homogenized in 1 mL of PBS and centrifuged at 13,000×g for 10 min at 4 °C. The supernatant was collected, and the MPO activity was determined according to the manufacturer's instructions. MPO activity is expressed in units per gram of colonic tissue. One unit of MPO activity is defined as the amount of enzyme degrading 1 μmol of peroxide per minute at 25 °C. The concentrations of pro-inflammatory cytokines (IL-6 and TNF-α) in the colonic tissues were also measured by ELISA. The colonic tissues (50 mg) were homogenized in 1 mL of RIPA buffer containing protease inhibitors and centrifuged at 13,000×g for 10 min at 4 °C. The supernatant was collected, and the concentrations of IL-6 and TNF-α were measured using ELISA kits (Invitrogen, Waltham, MA, USA). The total protein concentration was determined by using a BCA protein assay kit (Thermo Fisher Scientific, Waltham, MA, USA).

2.18. Statistical analysis

All data are expressed as the mean ± standard deviation (SD). Statistical analyses were performed using Student's *t*-test or one-way ANOVA followed by Dunnett's test.

3. Results and discussion

3.1. Preparation and characterization of FA-AC

3.1.1. Physicochemical and structural characterization of FA-AC

FA-AC was prepared *via* an *in situ* sol−gel method as described in the Experimental section. FA-AC exhibited a narrow size distribution with an average size of 20.1 ± 3.5 nm and a zeta potential of 24.9 ± 1.4 mV. Since FA-AC is positively charged, it is capable of forming a nanocomplex with negatively charged proteins *via* an electrostatic interaction.

The structural characteristics of FA-AC were also examined by XRD analysis. As shown in Fig. 1A, both AC and FA-AC exhibited a broad d_{001} interlamellar reflection, and some broad higher angle in-plane peaks, implying that the structural framework of AC was well retained during the interaction with FA. FA-AC displayed a characteristic diffraction peak (d_{060}) of approximately $2\theta = 59°$, corresponding to the 2:1 trioctahedral smectite structure[45], similar to AC. Furthermore, FA-AC showed a low-angle d_{001} interlayer spacing of 1.47 nm, consistent with interlayer spacing of AC, implying an interaction between FA and the surface of AC lamellae rather than intercalation of FA into the interlayer space of AC. The stacked lamellar structure of FA-AC was also confirmed using TEM (Fig. 1B). In particular, the observed lamellar structure of FA-AC indicated an interlayer distance of 1.47 nm, which is consistent with the results from the XRD analysis.

The structural characteristics of FA-AC were also examined by FT-IR analysis. As shown in Fig. 1C, the FT-IR spectrum of AC showed characteristic peaks of aminopropyl groups (Si−C, 1125 cm^{-1}; N−H, 1607 cm^{-1}) and the phyllosilicate framework (Si−O−Si, 1030 cm^{-1}; Mg−O, Mg−O−Si, 565−500 cm^{-1})[46,47]. On the other hand, FA displayed peaks at 1605, 1690, and 1485 cm^{-1}, corresponding to N−H bending vibration of the CONH group, C=O stretching of carboxyl group, and the absorption band of phenyl ring, respectively[48]. In the case of FA-AC, the peak corresponding to N−H groups at 1607 cm^{-1} shifted to 1614 cm^{-1}. In addition, there was the peak shift from 1690 cm^{-1}−1680 cm^{-1} since the hydrogen bond formation between C=O of FA and N−H of AC decreased the electron density of C=O due to electronic charge transfer from C=O to the N−H antibonding orbital, thus lowering its vibrational frequency[49,50]. These results from the FT-IR analysis further support the observations of the XRD analysis, suggesting intermolecular interactions between FA and aminopropyl moieties on the surface of AC.

The cytotoxicity of FA-AC was examined in Caco-2 cells and RAW264.7 cells. As shown in Fig. 1D, FA-AC did not show any cytotoxicity even at high concentrations up to 1000 μg/mL in both Caco-2 cells and RAW264.7 cells.

Taken together, FA-AC was prepared *via* a simple *in situ* sol−gel method, and it may be useful as a drug delivery carrier since it exhibited favorable profiles in terms of cytotoxicity, stability, and capability to form a nanocomplex with negatively charged macromolecules.

3.1.2. Cellular uptake characteristics of FA-AC

FR-β-positive macrophages are abundant in many autoimmune diseases including Crohn's disease and ulcerative colitis; however, FR-β is not expressed in resting macrophages or any other healthy tissues[51,52]. Therefore, in the present study, the cellular uptake characteristics of FA-AC-based nanocomplex were evaluated in RAW264.7 cells with/without LPS activation and were compared to that of AC-based nanocomplex, a non-targeted carrier. For the bio-imaging assay, fluorescence-labeled nanocomplex containing FITC-BSA (EFA-AC-FITC-BSA and EAC-FITC-BSA) were fabricated and their intracellular uptake profiles were examined using confocal laser scanning microscopy and flow cytometry.

As shown in Fig. 2A, LPS treatment induced the M1 polarization of RAW264.7 cells[51,52], highly enhancing the expression of FR-β. LPS-stimulated cells exhibited approximately 3.5-fold higher expression of FR-β than cells without LPS-stimulation. Accordingly, the cellular uptake of EFA-AC-FITC-BSA was significantly enhanced in LPS-stimulated cells (Fig. 2B). Furthermore, while the cellular uptake of EFA-AC-FITC-BSA in control cells without LPS-activation was not affected by pretreatment with free FA, it was significantly decreased in LPS-stimulated cells by pretreatment with free FA (Fig. 2B). These results suggest that FR-β could be involved in the cellular uptake of the FA-AC-based nanocomplex. In contrast, the cellular uptake of non-targeted AC-based nanocomplex (EAC-FITC-BSA) was not affected by the expression level of FR-β (Fig. 2B). These findings are also consistent with the observation from the bio-imaging assay using CLSM. As shown in Fig. 2C, the cellular uptake of targeted and non-targeted nanoparticles was similar in control cells without LPS-stimulation. However, the cellular uptake of EFA-AC-FITC-BSA was significantly higher than that of non-targeted EAC-FITC-BSA in the LPS-stimulated cells; this was dramatically diminished by pretreatment with free FA.

Taken together, these results suggest that the FA-AC-based nanocomplex underwent FR-β-mediated endocytosis. These results support that this FA-AC-based nanocomplex should be effective at targeting activated macrophages overexpressing FR-β in the inflamed colon.

3.1.3. Ex vivo colonic distribution study

Improving effective drug delivery to the inflamed tissues is one of the most important features of nanomedicines used in the treatment of inflammatory bowel diseases. Thus, the effectiveness of a pH-responsive FA-AC-based nanocomplex as a site-selective drug delivery system was evaluated in mice. First, after oral administration of fluorescence-labeled nanocomplex (EFA-AC-FITC-BSA) to mice, the gastrointestinal (GI) distribution of fluorescence-labeled nanoparticles was examined by using an *in vivo* imaging system (Supporting Information Fig. S1). At 3 h post-dose, strong fluorescence signals were observed in the upper GI tract. However, at 12 h post-dose, EFA-AC-based nanocomplex achieved much greater colonic distribution of FITC-BSA while the fluorescence intensity in upper GI tract decreased significantly (Fig. S1). The colonic absorption of fluorescence-labeled nanoparticles was also evaluated in DSS-induced colitis mice compared with healthy mice. After oral administration of targeted and non-targeted nanocomplex (EFA-AC-FITC-BSA and EAC-FITC-

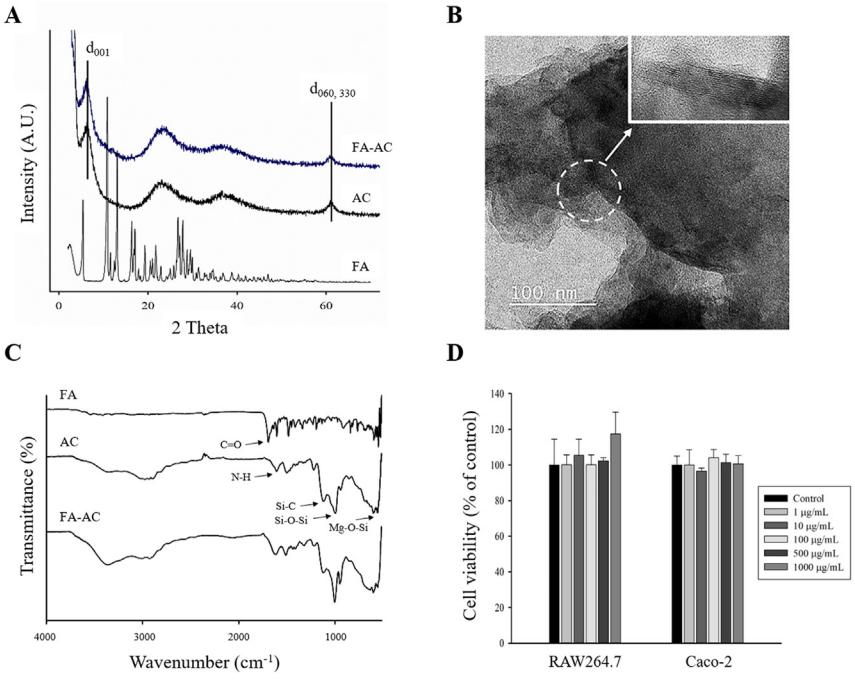

Figure 1 *In vitro* characterization of FA-AC (A) XRD patterns of FA, AC, and FA-AC (B) TEM image of FA-AC (C) FT-IR spectra of FA, AC, and FA-AC (D) Cytotoxicity of FA-AC in Caco-2 and RAW264.7 cells (mean ± SD, $n = 5$).

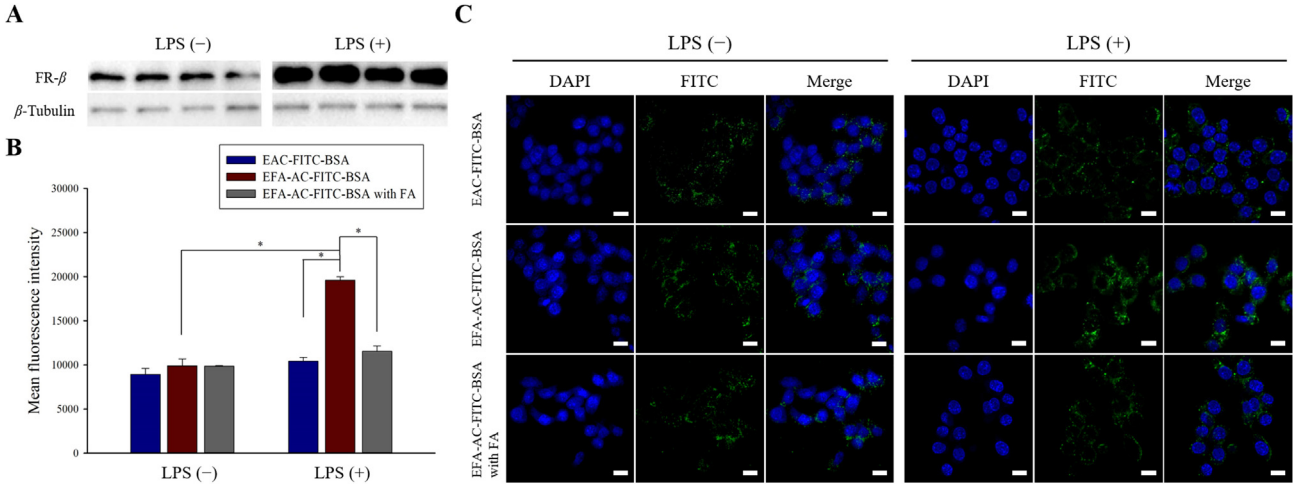

Figure 2 (A) Expression of FR-β in RAW264.7 cells with/without LPS-stimulation (B) Cellular uptake of nanocomplex in RAW264.7 cells with/without LPS-stimulation (mean ± SD, $n = 3$), $^*P < 0.001$ (C) CLSM images of the intracellular uptake of nanocomplex in RAW264.7 cells with/without LPS-stimulation. The scale bar indicates 10 μm.

BSA), the accumulations of nanoparticles in the inflamed colon and the healthy colon were examined with a bioimaging assay. As shown in Fig. 3A, both EFA-AC-FITC-BSA and EAC-FITC-BSA exhibited much stronger fluorescence signals in the inflamed colonic tissues than in the healthy colonic tissues, indicating more effective colonic absorption of nanoparticles in the inflamed tissues. This result may be explained by several factors. First, due to the dissolution of Eudragit® S100 at a pH above 7.0, the pH-dependent coating layer could minimize premature drug release in the upper GI tract and protect the entrapped proteins from proteolytic degradation, resulting in more efficient delivery of intact proteins to the colon. Second, the pathophysiological changes in inflamed tissues including the disruption of the colonic epithelium and the loss of barrier integrity of tight junctions should increase the penetration of nanoparticles across the colonic epithelium[53,54]. In addition, as reported in previous studies[55,56], the enhanced mucus secretion in ulcerative colitis may increase the residence time of nanoparticles in the inflamed colon. After removal of the Eudragit® S100 coating layer, the released nanocomplex had positive charges and could interact with negatively charged colonic mucins, increasing the residence time of nanoparticles in the inflamed tissues. Particularly, FA-AC-based nanocomplex achieved approximately 2-fold higher colonic absorption than

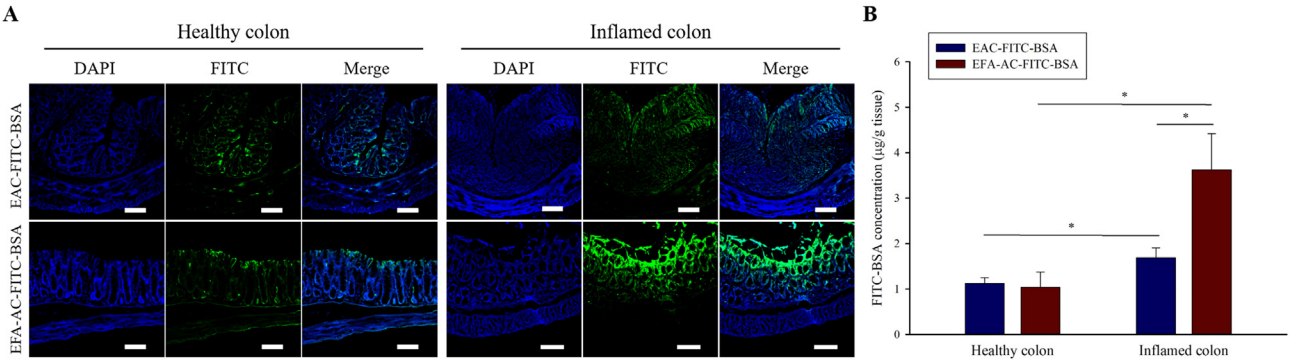

Figure 3 *Ex vivo* colonic absorption study of fluorescence-labeled nanocomplex in DSS-induced colitis mice and healthy mice. Colonic tissues were obtained 12 h after oral administration of each nanocomplex to mice. The dose was equivalent to 10 mg/kg of FITC-BSA (A) Confocal images of excised healthy and inflamed colonic tissues (scale bar is 100 μm). (B) Quantitative determination of FITC-BSA in healthy and inflamed colonic tissues (mean ± SD, $n = 4$). *$P < 0.05$.

non-targeted AC-based nanocomplex in the inflamed colons as confirmed by quantitative fluorescence analysis (Fig. 3B). This result may be explained by the influx of activated FR-β-positive macrophages into the colons of colitis mice.

Taken together, these results suggest that this pH-responsive FA-AC-based nanocomplex should be effective in facilitating drug delivery to the inflamed colon in colitis mice.

3.2. *Application of FA-AC for the oral delivery of IFX*

3.2.1. *Physicochemical and structural characterization of IFX-loaded nanocomplex*

A pH-responsive FA-AC-based nanocomposite system of IFX (EFA-AC-IFX) was fabricated for the effective oral delivery of monoclonal antibodies to the inflamed colon. The drug-loaded core nanocomplex (FA-AC-IFX) was prepared *via* the electrostatic interaction of IFX with FA-AC and then coated with Eudragit® S100 (EFA-AC-IFX). As summarized in Table 1, FA-AC-IFX was obtained with the average size of 140 ± 1.3 nm and high entrapment efficiency (>94%). Given that the isoelectric point (pI) of IFX is 7.6[57], IFX is negatively charged at a pH above 7.6, leading to the formation of a nanocomplex between IFX and positively charged FA-AC *via* electrostatic interactions. The zeta potential of FA-AC-IFX was 3.25 ± 0.06 mV, implying that the surface of IFX might be fully masked by the adsorption of FA-AC in nanocomplex (Table 1). Subsequently, the positive charge of FA-AC-IFX facilitated the deposition of the pH-sensitive polymer (Eudragit® S100) for surface coating, resulting in a size increase and reversal of the surface charge (the particle size and zeta potential of EFA-AC-IFX were 384 ± 10.3 nm and −13.6 ± 0.6 mV, respectively).

The morphology of the nanocomplex was also examined by TEM. As shown in Fig. 4A, both FA-AC-IFX and EFA-AC-IFX were spherical in shape and exhibited particle sizes comparable to those measured by dynamic light scattering. The formation of a drug-loaded nanocomplex was also confirmed by FT-IR analysis. As shown in Fig. 4B, the FT-IR spectrum of FA-AC-IFX displayed a strong absorbance band at 1639 cm^{-1} from the β-sheet band of IFX[58] as well as bands of Si−O−Si at 1020 cm^{-1} and Mg−O−Si at 565−497 cm^{-1} from the phyllosilicate framework of AC[59], suggesting the integration of IFX and FA-AC into the nanocomplex. In the case of EFA-AC-IFX, the FT-IR spectrum exhibited peaks from Eudragit® S100, including −C−O− stretching vibration at 1150 cm^{-1}, a $-CH_3$ bend at 1450 cm^{-1}, and −C=O stretching at 1727 cm^{-1} [60,61], in addition to the peaks from IFX and AC (Fig. 4B), confirming the incorporation of the Eudragit® S100 component.

Since structural instability can affect the biological activity of antibodies, the conformational stability of IFX entrapped in the FA-AC-based nanocomplex was evaluated by CD analysis and SDS-PAGE. As shown in Fig. 4C, the CD spectra of IFX released from the FA-AC-based nanocomplex nearly overlapped with that of native IFX and exhibited a strong negative band at 218 nm, indicating the typical β-sheet structure of IFX[62,63]. The results from SDS-PAGE also confirmed the stability of IFX entrapped in the nanocomplex. As shown in Fig. 4D, IFX entrapped in the FA-AC-based nanocomplex displayed a single band at a molecular weight of ≈150 kDa, similar to native IFX[64]. These results suggest that the structural stability of IFX is well maintained inside nanocomposite systems.

3.2.2. *Protection against enzymes and gastric acid degradation*

During oral delivery, the GI stability of antibodies is crucial for retaining their biological activity. Since antibodies are easily destabilized by the acidic gastric fluids and proteolytic enzymes in the GI tract, the structural stability of IFX entrapped in EFA-AC-

Table 1 Characterization of nanocomposite formulations (mean ± SD, $n = 3$).

Formulation	Size (nm)	PDI	Zeta potential (mV)	EE (%)
FA-AC	20.1 ± 3.5	0.324 ± 0.034	24.9 ± 1.4	NA
FA-AC-IFX	140 ± 1.3	0.342 ± 0.031	3.25 ± 0.06	94.6 ± 1.0
EFA-AC-IFX	384 ± 10.3	0.426 ± 0.051	−13.6 ± 0.6	87.0 ± 1.4

NA, not applicable.

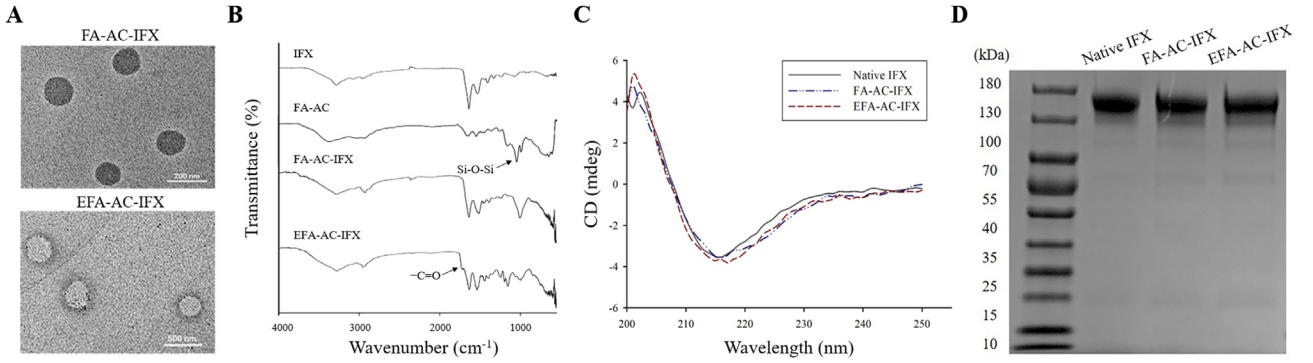

Figure 4 Characterization of drug-loaded nanoparticles. (A) TEM images of FA-AC-IFX and EFA-AC-IFX, (B) FT-IR spectra of IFX, FA-AC, FA-AC-IFX, and EFA-AC-IFX, (C) CD spectra of IFX released from nanocomplex in pH 7.4 PBS, and (D) SDS-PAGE of IFX released from nanocomplex in pH 7.4 PBS.

IFX was evaluated in simulated gastric fluid (SGF) and simulated intestinal fluid (SIF) containing proteolytic enzymes by using CD spectroscopy and SDS-PAGE. As shown in Fig. 5A, IFX entrapped in EFA-AC-IFX exhibited a spectral pattern comparable to that of the control (native IFX) in both SGF and SIF, implying that the conformational stability of IFX in nanoparticles could be well retained despite gastric acidity and proteolytic enzymes. This protective effect of EFA-AC-IFX on the GI stability of antibodies was also confirmed with SDS-PAGE. As shown in Fig. 5B, IFX released from EFA-AC-IFX displayed only a single band (molecular weight of ≈150 kDa), similar to native IFX, without any additional bands from fragmentation or aggregation in SGF and SIF. The protective effect of EFA-AC-IFX against enzymatic degradation may be explained by several factors. First, the outer coating layer of Eudragit® S100 was not dissolved in acidic conditions, preventing the exposure of IFX to the proteolytic enzymes in SGF. Even after removal of the outer coating layer in SIF, the formation of a core complex between FA-AC and IFX kept antibodies embedded in FA-AC matrix, thereby preventing proteolytic enzymes from accessing the antibodies. Taken together, the results suggest that EFA-AC-IFX should be effective in protecting antibodies in the harsh GI environment.

3.2.3. *In vitro drug release*

The release profiles of IFX from the nanocomplex were evaluated using a pH-changing buffer solution to reflect the pH variation in the GI tracts of patients with colitis[40,42,65]. At pH 1.2, FA-AC-IFX achieved rapid drug release of approximately 95% within 1 h, while EFA-AC-IFX exhibited minimal drug release (<10%) because the outer coating layer of Eudragit® S100 is insoluble in acidic conditions (Fig. 6). After increasing the pH to 7.2, drug release from EFA-AC-IFX was facilitated and increased to approximately 48% due to dissolution of the outer coating layer at this pH. Then, the pH was changed to 5.5 to reflect the pH of the inflamed colon, and EFA-AC-IFX displayed continuous drug release, achieving an additional 40% of drug release. This result may be explained by the electrostatic repulsion between IFX and FA-AC at pH 5.5. Considering that the isoelectric point of IFX is 7.6[57], IFX could be positively charged at pH 5.5; thus, there might be electrostatic repulsion between IFX and positively charged FA-AC, facilitating drug release from the nanocomplex. The pH-dependent drug release profile of EFA-AC-IFX should be beneficial as it can protect IFX from the acidic environment of the stomach and deliver the majority of IFX to the colon.

3.2.4. *In vivo efficacy studies*

The anti-inflammatory effects of orally administered EFA-AC-IFX compared to oral IFX solution were evaluated in DSS-induced colitis mice. As summarized in Fig. 7, the therapeutic effectiveness was monitored in various aspects including body weight loss, change in colon length, disease activity index (DAI), and histopathological examination. Overall, the oral administration of free

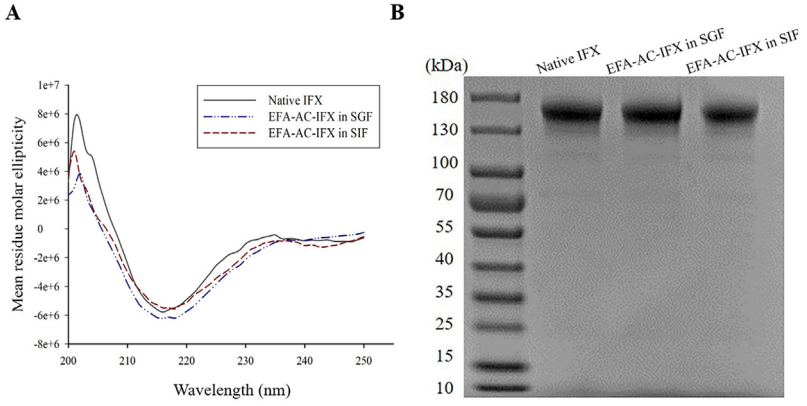

Figure 5 CD spectra (A) and SDS-PAGE (B) of native IFX and IFX released from the nanocomplex after incubation of EFA-AC-IFX in SGF and SIF for 2 h.

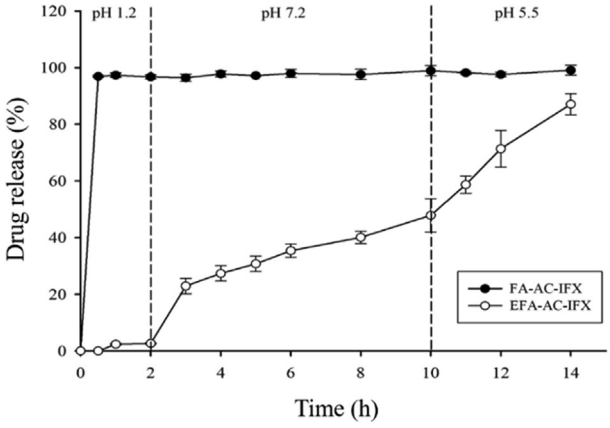

Figure 6 Drug release profiles from the nanocomplex at different pHs (mean ± SD, $n = 3$).

IFX solution did not show any therapeutic efficacy in DSS-induced colitis mice; this may be due to the almost complete destabilization of IFX in the GI tract. In contrast, EFA-AC-IFX exhibited a significant protective effect against the progression of inflammation. First, the effect on body weight loss, an important parameter for monitoring the severity of colitis, was examined (Fig. 7A). While DSS-induced colitis mice showed significant body weight loss to approximately 70% of their initial weights, those treated with oral administration of EFA-AC-IFX did not show any significant weight loss. There was also significantly greater improvement in the DAI in the EFA-AC-IFX treatment group than in the oral IFX solution or other treatment groups (Fig. 7B). Diarrhea and bloody stools were observed in DSS-induced colitis mice but not in mice treated with EFA-AC-IFX. Furthermore, EFA-AC-IFX exhibited a significant protective effect against colon length reduction. There was no significant difference in colon length between mice in the EFA-AC-IFX treatment group and control group (healthy mice), while mice in

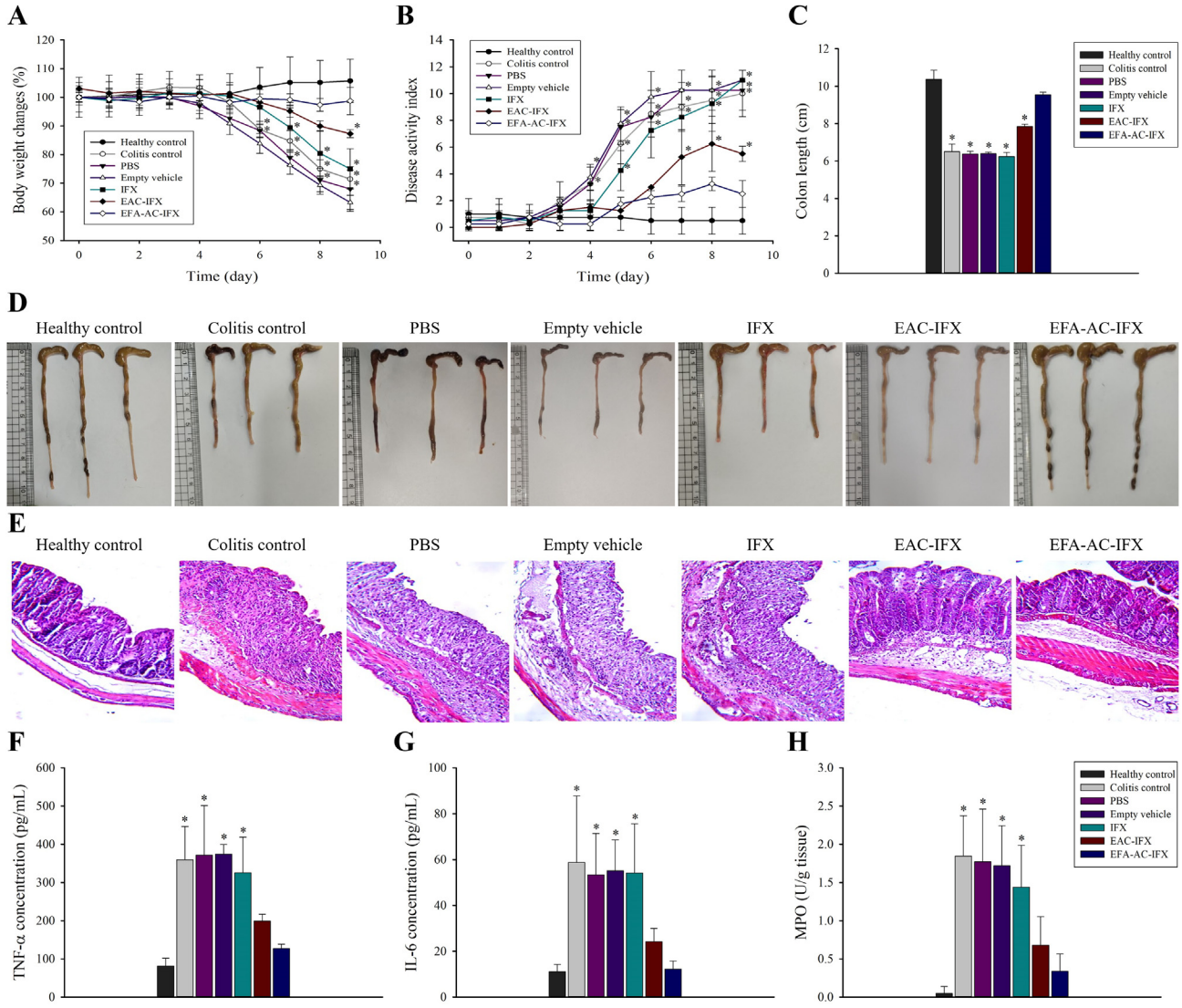

Figure 7 *In vivo* therapeutic effects of orally administered EFA-AC-IFX in DSS-induced colitis mice. The *in vivo* efficacy in each treatment group was assessed by changes in body weight (A), DAI (B), colon length (C, D), H&E staining of colonic sections (E), secretion of TNF-α (F) and IL-6 (G), and MPO activity (H). Values are expressed as the mean ± SD, $n = 4$/group. *$P < 0.01$ compared with the healthy control group.

the other treatment groups displayed significant colon shortening (Fig. 7C and D). Histological evaluation of the colonic tissues also confirmed the therapeutic potential of EFA-AC-IFX. As shown in Fig. 7E, the EFA-AC-IFA treatment group demonstrated morphological tissue structures resembling those of healthy mouse tissue and did not show any significant signs of microscopic inflammation. In contrast, colonic tissues from the colitis control group exhibited robust signs of inflammation including epithelial erosion, interstitial edema, and infiltration of inflammatory cells (Fig. 7E).

Since pro-inflammatory cytokines such as TNF-α and IL-6 directly drive colonic tissue damage *via* enhancing apoptosis of colonic epithelial cells and promoting the infiltration and activation of immune cells[66], the effect of IFX-loaded nanocomplex on the secretion of TNF-α and IL-6 was examined using ELISA. As summarized in Fig. 7F and G, EFA-AC-IFX treatment significantly suppressed the secretion of TNF-α and IL-6, while DSS-induced colitis mice exhibited high levels of these inflammatory cytokines. Furthermore, the MPO activity in colonic tissues was significantly lower in the EFA-AC-IFX treatment group than in the other treatment groups (Fig. 7H). These results suggest that orally administered EFA-AC-IFX could effectively alleviate symptoms of colitis in mice *via* suppressing the secretion of pro-inflammatory cytokines and colonic MPO activity. Non-targeted EAC-IFX also exhibited *in vivo* efficacy to a certain extent, particularly in terms of some parameters including colon length, secretion of inflammatory cytokines, and colonic MPO activity, although its efficacy was lower than that of targeted nanocomplex.

Taken together, orally administered EFA-AC-IFX was effective in alleviating the progression of ulcerative colitis, while oral IFX solution had no efficacy. There are several hypotheses for the good *in vivo* efficacy of orally administered EFA-AC-IFX. First, EFA-AC-IFX should increase the local drug delivery of nanoparticles to the inflamed colon. As shown in Fig. 3, FA-AC-based nanoparticles could concentrate, to a greater extent, in the area of inflammation than non-targeted nanoparticles. Furthermore, after the dissolution of Eudragit® S100 coating layer at pH above 7.0, positively charged nanoparticles (FA-AC-IFX) can interact with negatively charged colonic mucins, prolonging the residence time of nanoparticles in the inflamed tissues[67]. Second, after the colonic absorption, IFX can be released, to a certain extent, from nanoparticles in lamina propria and then the released IFX may interact with soluble and membrane TNF-α, contributing to the *in vivo* efficacy. In addition, FA-AC itself has anti-inflammatory effect, reducing the secretion of pro-inflammatory cytokines and providing the synergistic effect (Supporting Information Fig. S2). Finally, the internalized IFX *via* FR-β-mediated endocytosis may contribute to alleviate the symptoms of colitis *via* the additional mechanisms beyond TNF-α neutralization. The mechanism of action of IFX other than TNF-α binding has been examined in many previous studies and emerging evidence suggests various mechanisms in addition to TNF-α neutralization[31–34]. Furthermore, since activated macrophages release various cytokines and reactive oxygen species that accelerate tissue damage[51], the internalized IFX may contribute to the modulation of these activated macrophages for the control of disease symptoms, which should be clarified in further studies.

In summary, the pH-dependent dissolution of the outer coating layer in EFA-AC-IFX allowed retention of the structural integrity of antibodies in the GI tract and enabled more effective release of antibody-loaded FA-AC core nanocomplex into the colonic lumen. Consequently, oral administration of EFA-AC-IFX could significantly decrease the secretion of pro-inflammatory cytokines and alleviate the symptoms of colitis in mice. These results suggest that EFA-AC-IFX should be a promising site-selective oral delivery system of IFX for the treatment of ulcerative colitis.

4. Conclusions

In the present study, a pH-responsive FA-AC-based nanocomplex was developed for effective oral and site-selective delivery of therapeutic antibodies. *In vitro and ex vivo* studies demonstrated that this pH-responsive FA-AC-based nanocomplex was successful to achieve protection of the structural integrity of antibodies during the passage through the GI tract and more preferential accumulation in the inflamed colon. Consequently, oral administration of IFX-loaded nanocomplex (EFA-AC-IFX) effectively alleviated the symptoms of colitis in DSS-induced colitis mice, while oral IFX solution had no efficacy. Given that (i) this FA-AC-based organic/inorganic hybrid nanocomposite system is applicable to diverse protein-based drugs, (ii) its preparation method is simple and easy, and (iii) it is orally available to improve patient compliance, this nanocomposite system may represent a new platform for site-selective oral delivery of various therapeutic antibodies in the treatment of many macrophage-mediated inflammatory diseases.

Acknowledgments

This research was supported by National Research Foundation of Korea (NRF), South Korea grant funded by the Korea government (MSIT) (Nos. 2019R1A2C2004873 and 2018R1A5A2023127) and the BK21 FOUR program through the National Research Foundation (NRF) funded by the Ministry of Education of Korea.

Author contributions

Hyo-Kyung Han designed the research and supervised the experiments. Sang Hoon Lee carried out the experiments and performed data analysis. Jae Geun Song participated part of the experiments and data analysis. Sang Hoon Lee and Jae Geun Song wrote the manuscript. Hyo-Kyung Han reviewed and edited the manuscript. All of the authors have read and approved the final manuscript.

Conflicts of interest

The authors have no conflicts of interest to declare.

Appendix A. Supporting information

Supporting data to this article can be found online at https://doi.org/10.1016/j.apsb.2022.06.006.

References

1. Awwad S, Angkawinitwong U. Overview of antibody drug delivery. *Pharmaceutics* 2018;**10**:83.
2. Ryman JT, Meibohm B. Pharmacokinetics of monoclonal antibodies. *CPT Pharmacomet Syst Pharmacol* 2017;**6**:576–88.
3. Ecker DM, Jones SD, Levine HL. The therapeutic monoclonal antibody market. *MAbs* 2015;**7**:9–14.
4. Anselmo AC, Gokarn Y, Mitragotri S. Non-invasive delivery strategies for biologics. *Nat Rev Drug Discov* 2019;**18**:19–40.

5. Johnson DE. Biotherapeutics: challenges and opportunities for predictive toxicology of monoclonal antibodies. *Int J Mol Sci* 2018;**19**:3685.
6. Matucci A, Vultaggio A, Danesi R. The use of intravenous *versus* subcutaneous monoclonal antibodies in the treatment of severe asthma: a review. *Respir Res* 2018;**19**:154.
7. Tashima T. Delivery of orally administered digestible antibodies using nanoparticles. *Int J Mol Sci* 2021;**22**:3349.
8. Durán-Lobato M, Niu Z, Alonso MJ. Oral delivery of biologics for precision medicine. *Adv Mater* 2020;**32**:1901935.
9. Mitragotri S, Burke PA, Langer R. Overcoming the challenges in administering biopharmaceuticals: formulation and delivery strategies. *Nat Rev Drug Discov* 2014;**13**:655−72.
10. Zelikin AN, Ehrhardt C, Healy AM. Materials and methods for delivery of biological drugs. *Nat Chem* 2016;**8**:997−1007.
11. Pabari RM, Mattu C, Partheeban S, Almarhoon A, Boffito M, Ciardelli G, et al. Novel polyurethane-based nanoparticles of infliximab to reduce inflammation in an *in-vitro* intestinal epithelial barrier model. *Int J Pharm* 2019;**565**:533−42.
12. Wang X, Yan J, Wang L, Pan D, Xu Y, Wang F, et al. Oral delivery of anti-TNF antibody shielded by natural polyphenol-mediated supramolecular assembly for inflammatory bowel disease therapy. *Theranostics* 2020;**10**:10808−22.
13. Kumeria T, Wang J, Kim B, Park JH, Zuidema JM, Klempner M, et al. Enteric polymer-coated porous silicon nanoparticles for site-specific oral delivery of IgA antibody. *ACS Biomater Sci Eng* 2020. Available from: https://doi.org/10.1021/acsbiomaterials.0c01313.
14. Maurer JM, Hofman S, Schellekens RCA, Tonnis WF, Dubois AOT, Woerdenbag HJ, et al. Development and potential application of an oral ColoPulse infliximab tablet with colon specific release: a feasibility study. *Int J Pharm* 2016;**505**:175−86.
15. Kim JM, Kim DH, Park HJ, Ma HW, Park IS, Son M, et al. Nanocomposites-based targeted oral drug delivery systems with infliximab in a murine colitis model. *J Nanobiotechnol* 2020;**18**:133.
16. Angsantikul P, Peng K, Curreri AM, Chua Y, Chen KZ, Ehondor J, et al. Ionic liquids and deep eutectic solvents for enhanced delivery of antibodies in the gastrointestinal tract. *Adv Funct Mater* 2020;**31**:2002912.
17. Carrillo-Conde BR, Brewer E, Lowman A, Peppas NA. Complexation hydrogels as oral delivery vehicles of therapeutic antibodies: an *in vitro* and *ex vivo* evaluation of antibody stability and bioactivity. *Ind Eng Chem Res* 2015;**54**:10197−205.
18. Prado MS, Bendtzen K, Andrade LEC. Biological anti-TNF drugs: immunogenicity underlying treatment failure and adverse events. *Expet Opin Drug Metabol Toxicol* 2017;**13**:985−95.
19. Patil AJ, Mann S. Self-assembly of bio-inorganic nanohybrids using organoclay building blocks. *J Mater Chem* 2008;**18**:4605−15.
20. Lee SH, Song JG, Han HK. Development of pH-responsive organic-inorganic hybrid nanocomposites as an effective oral delivery system of protein drugs. *J Control Release* 2019;**311−2**:74−84.
21. Song JG, Lee SH, Han HK. Development of an M cell targeted nanocomposite system for effective oral protein delivery: preparation, *in vitro* and *in vivo* characterization. *J Nanobiotechnol* 2021;**19**:15.
22. Lee SH, Back SY, Song JG, Han HK. Enhanced oral delivery of insulin *via* the colon-targeted nanocomposite system of organoclay/glycol chitosan/Eudragit®S100. *J Nanobiotechnol* 2020;**18**:104.
23. Han HK, Lee YC, Lee MY, Patil AJ, Shin HJ. Magnesium and calcium organophyllosilicates: synthesis and *in vitro* cytotoxicity study. *ACS Appl Mater Interfaces* 2011;**3**:2564−72.
24. Oh JM, Choi SJ, Lee GE, Han SH, Choy JH. Inorganic drug-delivery nanovehicle conjugated with cancer-cell-specific ligand. *Adv Funct Mater* 2009;**19**:1617−24.
25. Chandrupatla DMSH, Molthoff CFM, Lammertsma AA, van der Laken CJ, Jansen G. The folate receptor β as a macrophage-mediated imaging and therapeutic target in rheumatoid arthritis. *Drug Deliv Transl Res* 2019;**9**:366−78.
26. Elnakat H, Ratnam M. Role of folate receptor genes in reproduction and related cancers. *Front Biosci* 2006;**11**:506−19.
27. Van der Heijden JW, Oerlemans R, Dijkmans BAC, Qi H, van der Laken CJ, Lems WF, et al. Folate receptor β as a potential delivery route for novel folate antagonists to macrophages in the synovial tissue of rheumatoid arthritis patients. *Arthritis Rheum* 2009;**60**:12−21.
28. Xia W, Hilgenbrink AR, Matteson EL, Lockwood MB, Cheng JX, Low PS. A functional folate receptor is induced during macrophage activation and can be used to target drugs to activated macrophages. *Blood* 2009;**113**:438−46.
29. Sega EI, Low PS. Tumor detection using folate receptor-targeted imaging agents. *Cancer Metastasis Rev* 2008;**27**:655−64.
30. Billmeier U, Dieterich W, Neurath MF, Atreya R. Molecular mechanism of action of anti-tumor necrosis factor antibodies in inflammatory bowel diseases. *World J Gastroenterol* 2016;**22**:9300−13.
31. D'Haens G, Van Deventer S, Van Hogezand R, Chalmers D, Kothe C, Baert F, et al. Endoscopic and histological healing with infliximab anti-tumor necrosis factor antibodies in Crohn's disease: a European multicenter trial. *Gastroenterology* 1999;**116**:1029−34.
32. Suenaert P, Bulteel V, Lemmens L, Noman M, Geypens B, Assche G van, et al. Anti-tumor necrosis factor treatment restores the gut barrier in Crohn's disease. *Am J Gastroenterol* 2002;**97**:2000−4.
33. Assas MB, Levison SE, Little M, England H, Battrick L, Bagnall J, et al. Anti-inflammatory effects of infliximab in mice are independent of tumour necrosis factor α neutralization. *Clin Exp Immunol* 2017;**187**:225−33.
34. Guo Y, Lu N, Bai A. Clinical use and mechanisms of infliximab treatment on inflammatory bowel disease: a recent update. *BioMed Res Int* 2013;**2013**:581631.
35. Xiao Q, Li X, Li Y, Wu Z, Xu C, Chen Z, et al. Biological drug and drug delivery-mediated immunotherapy. *Acta Pharm Sin B* 2021;**11**:941−60.
36. Rutgeerts P, Van Assche G, Vermeire S. Review article: infliximab therapy for inflammatory bowel disease—seven years on. *Aliment Pharmacol Ther* 2006;**23**:451−63.
37. Wang S, Cao H, Zhong Y, Yang Y, Shao Z. A novel aminoclay-curcumin hybrid for enhanced chemotherapy. *J Mater Chem B* 2016;**4**:4295−301.
38. Pawar A, Singh S, Rajalakshmi S, Shaikh K, Bothiraja C. Development of fisetin-loaded folate functionalized pluronic micelles for breast cancer targeting. *Artif Cell Nanomed Biotechnol* 2018;**46**:347−61.
39. Khodaverdi E, Maftouhian S, Aliabadi A, Hassanzadeh-Khayyat M, Mohammadpour F, Khameneh B, et al. Casein-based hydrogel carrying insulin: preparation, *in vitro* evaluation and *in vivo* assessment. *J Pharm Investig* 2019;**49**:635−41.
40. Hua S, Marks E, Schneider JJ, Keely S. Advances in oral nano-delivery systems for colon targeted drug delivery in inflammatory bowel disease: selective targeting to diseased *versus* healthy tissue. *Nanomedicine* 2015;**11**:1117−32.
41. Beloqui A, Coco R, Memvanga PB, Ucakar B, Des Rieux A, Préat V. pH-Sensitive nanoparticles for colonic delivery of curcumin in inflammatory bowel disease. *Int J Pharm* 2014;**473**:203−12.
42. Oshi MA, Lee J, Naeem M, Hasan N, Kim J, Kim HJ, et al. Curcumin nanocrystal/pH-responsive polyelectrolyte multilayer core−shell nanoparticles for inflammation-targeted alleviation of ulcerative colitis. *Biomacromolecules* 2020;**21**:3571−81.
43. Seo DH, Che X, Kwak MS, Kim S, Kim JH, Ma HW, et al. Interleukin-33 regulates intestinal inflammation by modulating macrophages in inflammatory bowel disease. *Sci Rep* 2017;**7**:851.
44. Jeong S, Ju S, Park S, Jung Y. 5-[(3-Carboxy-4-hydroxyphenyl)diazenyl] nicotinic acid, an azo-linked mesalazine−nicotinic acid conjugate, is a colon-targeted mutual prodrug against dextran sulfate sodium-induced colitis in mice. *J Pharm Investig* 2021;**51**:317−25.
45. Ganayee MA, Manju CK, Dar WA, Mondal B, Pradeep T. Entrapping atomically precise clusters in cyclodextrin-functionalized aminoclay sheets: synthesis and enhanced luminescence. *Ind Eng Chem Res* 2020;**59**:12737−44.

46. Song HP, Lee Y, Bui VKH, Oh YK, Park HG, Kim MI, et al. Effective peroxidase-like activity of Co-aminoclay [CoAC] and its application for glucose detection. *Sensors* 2018;**18**:457.
47. Yang L, Shao Y, Han HK. Improved pH-dependent drug release and oral exposure of telmisartan, a poorly soluble drug through the formation of drug−aminoclay complex. *Int J Pharm* 2014;**471**:258−63.
48. Rana S, Shetake NG, Barick KC, Pandey BN, Salunke HG, Hassan PA. Folic acid conjugated Fe_3O_4 magnetic nanoparticles for targeted delivery of doxorubicin. *Dalton Trans* 2016;**45**:17401−8.
49. Martinez-Felipe A, Brebner F, Zaton D, Concellon A, Ahmadi S, Piñol M, et al. Molecular recognition *via* hydrogen bonding in supramolecular complexes: a Fourier transform infrared spectroscopy study. *Molecules* 2018;**23**:2278.
50. Dash SK, Dash SS, Chattopadhyay S, Ghosh T, Tripathy S, Mahapatra SK, et al. Folate decorated delivery of self assembled betulinic acid nano fibers: a biocompatible anti-leukemic therapy. *RSC Adv* 2015;**5**:24144−57.
51. Hu Y, Wang B, Shen J, Low SA, Putt KS, Niessen HWM, et al. Depletion of activated macrophages with a folate receptor-beta-specific antibody improves symptoms in mouse models of rheumatoid arthritis. *Arthritis Res Ther* 2019;**21**:143.
52. Han W, Zaynagetdinov R, Yull FE, Polosukhin VV, Gleaves LA, Tanjore H, et al. Molecular imaging of folate receptor β-positive macrophages during acute lung inflammation. *Am J Respir Cell Mol Biol* 2015;**53**:50−9.
53. Digby-Bell JL, Atreya R, Monteleone G, Powell N. Interrogating host immunity to predict treatment response in inflammatory bowel disease. *Nat Rev Gastroenterol Hepatol* 2020;**17**:9−20.
54. Landy J, Ronde E, English N, Clark SK, Hart AL, Knight SC, et al. Tight junctions in inflammatory bowel diseases and inflammatory bowel disease associated colorectal cancer. *World J Gastroenterol* 2016;**22**:3117−26.
55. Li X, Lu C, Yang Y, Yu C, Rao Y. Site-specific targeted drug delivery systems for the treatment of inflammatory bowel disease. *Biomed Pharmacother* 2020;**129**:110486.
56. Fyderek K, Strus M, Kowalska-Duplaga K, Gosiewski T, Wędrychowicz A, Jedynak-Wąsowicz U, et al. Mucosal bacterial microflora and mucus layer thickness in adolescents with inflammatory bowel disease. *World J Gastroenterol* 2009;**15**:5287−94.
57. Goyon A, Excoffier M, Janin-Bussat MC, Bobaly B, Fekete S, Guillarme D, et al. Determination of isoelectric points and relative charge variants of 23 therapeutic monoclonal antibodies. *J Chromatogr B Anal Technol Biomed Life Sci* 2017;**1065−6**:119−28.
58. Saleem R, Cantin G, Wikström M, Bolton G, Kuhns S, McBride HJ, et al. Analytical and functional similarity assessment of ABP 710, a biosimilar to infliximab reference product. *Pharm Res* 2020;**37**:114.
59. Yang L, Choi SK, Shin HJ, Han HK. 3-Aminopropyl functionalized magnesium phyllosilicate as an organoclay-based drug carrier for improving the bioavailability of flurbiprofen. *Int J Nanomed* 2013;**8**:4147−55.
60. Vlachou M, Kikionis S, Siamidi A, Kyriakou S, Tsotinis A, Ioannou E, et al. Development and characterization of eudragit®-based electrospun nanofibrous mats and their formulation into nanofiber tablets for the modified release of furosemide. *Pharmaceutics* 2019;**11**:480.
61. Mehta R, Chawla A, Sharma P, Pawar P. Formulation and *in vitro* evaluation of Eudragit S-100 coated naproxen matrix tablets for colon-targeted drug delivery system. *J Adv Pharm Technol Res* 2013;**4**:31−41.
62. Joshi V, Shivach T, Yadav N, Rathore AS. Circular dichroism spectroscopy as a tool for monitoring aggregation in monoclonal antibody therapeutics. *Anal Chem* 2014;**86**:11606−13.
63. Chen K, Long DS, Lute SC, Levy MJ, Brorson KA, Keire DA. Simple NMR methods for evaluating higher order structures of monoclonal antibody therapeutics with quinary structure. *J Pharm Biomed Anal* 2016;**128**:398−407.
64. Gurjar SA, Wheeler JX, Wadhwa M, Thorpe R, Kimber I, Derrick JP, et al. The impact of thioredoxin reduction of allosteric disulfide bonds on the therapeutic potential of monoclonal antibodies. *J Biol Chem* 2019;**294**:19616−34.
65. Kim HY, Cheon JH, Lee SH, Min JY, Back SY, Song JG, et al. Ternary nanocomposite carriers based on organic clay-lipid vesicles as an effective colon-targeted drug delivery system: preparation and *in vitro/in vivo* characterization. *J Nanobiotechnol* 2020;**18**:17.
66. Jang DI, Lee AH, Shin HY, Song HR, Park JH, Kang TB, et al. The role of tumor necrosis factor alpha (TNF-α) in autoimmune disease and current TNF-α inhibitors in therapeutics. *Int J Mol Sci* 2021;**22**:2719.
67. Zhang W, Michalowski CB, Beloqui A. Oral delivery of biologics in inflammatory bowel disease treatment. *Front Bioeng Biotechnol* 2021;**9**:675194.